



University of
Massachusetts
Amherst

DOSE CALCULATIONS FOR [131I] META- IODOBENZYLGUANIDINEINDUCED BYSTANDER EFFECTS

Item Type	Article
Authors	Gow, M.D.;Seymour, CB;Boyd, M.;Mairs, RJ;Prestiwch, WV;Mothersill, CE
Download date	2026-05-20 16:15:19
Link to Item	https://hdl.handle.net/20.500.14394/20401

DOSE CALCULATIONS FOR [¹³¹I] META-IODOBENZYLGUANIDINE-INDUCED BYSTANDER EFFECTS

M. D. Gow¹, C. B. Seymour¹, M. Boyd², R. J. Mairs^{2,3}, W. V. Prestiwch¹, and C. E. Mothersill¹ □ ¹Medical Physics and Applied Radiation Sciences Department, McMaster University, Hamilton, Ontario, Canada L8S 4K1; ²Targeted Therapy Group, Division of Cancer Science and Molecular Pathology, Glasgow University, Cancer Research United Kingdom Beatson Laboratories, Glasgow, United Kingdom; ³Department of Child Health, Yorkhill Hospital, Glasgow, United Kingdom

□ Targeted radiotherapy is a potentially useful treatment for some cancers and may be potentiated by bystander effects. However, without estimation of absorbed dose, it is difficult to compare the effects with conventional external radiation treatment. Methods: Using the Vynckier – Wambersie dose point kernel, a model for dose rate evaluation was created allowing for calculation of absorbed dose values to two cell lines transfected with the noradrenaline transporter (NAT) gene and treated with [¹³¹I]MIBG. Results: The mean doses required to decrease surviving fractions of UVW/NAT and EJ138/NAT cells, which received medium from [¹³¹I]MIBG-treated cells, to 25 - 30% were 1.6 and 1.7 Gy respectively. The maximum mean dose rates achieved during [¹³¹I]MIBG treatment were 0.09 - 0.75 Gy/h for UVW/NAT and 0.07 - 0.78 Gy/h for EJ138/NAT. These were significantly lower than the external beam gamma radiation dose rate of 15 Gy/h. In the case of control lines which were incapable of [¹³¹I]MIBG uptake the mean absorbed doses following radiopharmaceutical were 0.03 - 0.23 Gy for UVW and 0.03 - 0.32 Gy for EJ138. Conclusion: [¹³¹I]MIBG treatment for ICCM production elicited a bystander dose-response profile similar to that generated by external beam gamma irradiation but with significantly greater cell death.

Key words: radiation bystander effect, MIBG, gene therapy, targeted radiotherapy, Vynckier - Wambersie

1. INTRODUCTION

Radiation therapy as a primary or adjunct procedure is used in approximately 60% of all cancer patients (Perez and Brady 1998). The purpose of this treatment is to deliver a lethal dose of radiation to a tumour site while sparing as much healthy tissue as possible. Targeted radiotherapy seeks to deliver a lethal dose of radiation to tumours while minimizing damage to normal organs (Boyd *et al.* 2004, Kufe and Weichselbaum 2003, Mitrofanova *et al.* 2006, Mairs and Boyd 2003). Radiolabelled [¹³¹I] *meta*-iodobenzylguanidine (MIBG), a low-LET β -par-

Address correspondence to Dr. Carmel E. Mothersill, Medical Physics and Applied Radiation Sciences Department, McMaster University, 1280 Main Street West, Hamilton, Ontario, Canada L8S 4K1. Tel: + 1.905.525.9140 x26227; Fax: + 1.905.522.5982; Email: mothers@mcmaster.ca

ticle emitter, is used for the diagnosis and treatment of patients with tumours derived from the neural crest (Cunningham *et al.* 2000, Mairs 1999). An analog of adrenergic neuron blockers (Wieland *et al.* 1980), MIBG is actively taken up via the noradrenaline transporter (NAT) – a high affinity, saturable and ATPase-dependent mechanism (Jacques *et al.* 1984, Mairs and Boyd 2008).

Heterogeneous uptake of [^{131}I]MIBG by tumours is an obstacle to a cure. This may be overcome by cross-fire irradiation of untargeted cells from neighbouring cells which have concentrated the radiopharmaceutical. However, collateral damage may also derive from radiation-induced biological bystander effects (RIBBE). RIBBE induced by [^{131}I]MIBG were examined by measurement of surviving fraction of recipient cells following irradiated-cell conditioned medium (ICCM) transfer (Boyd *et al.* 2006), originally developed by Mothersill and Seymour (1997). These results indicate substantial bystander cell kill. Unfortunately the survival data were presented as a function of activity concentration rather than absorbed dose. This causes difficulty in comparing RIBBE capability with previous estimates.

Therefore, this work sought to develop a dosimetric model for calculating absorbed dose to donor cells used in the creation of ICCM following treatment with [^{131}I]MIBG. This was accomplished through utilization of the Vynckier-Wambersie point source dose distribution (Vynckier and Wambersie 1982) applied to the appropriate geometry. Two separate models were developed and compared to determine the most computationally efficient method to perform calculation of absorbed dose over a range of applied activity concentration. For UVW and EJ138 cell lines used by Boyd *et al.* (2006), dose rate and absorbed values were calculated for each activity concentration applied. Following this, a re-examination of survival fraction data was undertaken comparing [^{131}I]MIBG and external beam radiation with respect to bystander cell death response.

2. MATERIALS AND METHODS

Experimental procedures utilized for assessment of recipient bystander cell death (i.e. surviving fraction) following treatment with ICCM generated from donor cell exposure to [^{131}I]MIBG were previously described in detail (Boyd *et al.* 2006).

2.1 Cell lines

Cell line hosts utilized were the UVW human glioma cell line (Boyd *et al.* 2004) and the EJ138 human bladder carcinoma cell line (Fullerton *et al.* 2005) and were maintained in 75-cm² flasks containing Eagle's MEM with 25 mmol/L N-(2-hydroxy-ethyl)piperazine-N9-(2-ethanesulfonic acid) buffer and Earle's Salt, supplemented with 10% (v/v) fetal bovine serum, penicillin/streptomycin (100 U/mL), fungizone (2 mg/mL),

L-glutamine (2 mmol/L), and nonessential amino acids (0.1 mmol/L). Cells were cultured at 37°C in a 5% CO₂ atmosphere. As UVW and EJ138 do not naturally express NAT required for active MIBG uptake, both cell lines were transfected according to previously described methods (Fullerton *et al.* 2005, Boyd *et al.* 1999). Cell size was determined using a Model TT Cell Counter and Analyzer System (Scharfe System, RJM Sales, NJ, USA). More than 10,000 cells were counted per measurement resulting in a mean ± SD diameter of 16.5 ± 0.9 µm and 12.8 ± 0.7 µm for UVW and EJ138 respectively. The doubling time was 18 hours for UVW and 17.5 hours for EJ138.

2.2 Uptake and Medium Transfer Experiments

Results of previous experiments indicated the administered and accumulated activity as a percentage of the activity in the incubation medium was 31.4% ± 3.7% for UVW/NAT cells and 21.4% ± 1.9% for EJ138/NAT cells with a linear relation between activity accumulated and administered (Boyd *et al.* 2006). The medium transfer technique has been described in detail in (Mothersill and Seymour 1997). Cells were initially seeded at 2 × 10⁵ cells per 25-cm² flask in 10 ml of complete medium and incubated for 24 h before irradiation. These cultures were 65 ± 5% confluent. Irradiated cells which produced conditioned medium (ICCM) were labelled “donors” while cells which received ICCM and not directly irradiated were labelled “recipients”. Irradiation of donor cells occurred by one of two methods:

1. Donor cells were irradiated by way of a ⁶⁰Co γ-ray source at a dose rate of 15 Gy/h through a range of doses from 0 to 9 Gy. Immediately following treatment, donor cells were returned to the incubator and maintained at 37°C and 5% CO₂ for one hour followed by removal of the medium (regardless of dose) which was passed through a 0.22-µm to ensure that no cell was present in the transferred medium (Mothersill and Seymour 1997). Medium was removed from recipient cells and replaced with the filtered ICCM. These recipient cells were then incubated and eventually seeded for clonogenic assay (Boyd *et al.* 2006). This experiment was performed 6 times in triplicate.
2. Donor cell medium was removed on the day of exposure and replaced with 1 ml of fresh medium. Cells were treated with activity concentrations of 0 to 11 MBq/ml of [¹³¹I]MIBG for 2 h as described previously (Boyd *et al.* 2004, Fullerton *et al.* 2005, Boyd *et al.* 1999, Mairs *et al.* 1995). This portion of the experiment was termed the “Uptake” phase. After 2 h, the donor medium was removed and cells are washed with PBS to eliminate unincorporated radiopharmaceutical. Five millilitres of fresh medium was then applied and the donor cells were placed back in the incubator for 1 h to allow for bystander factors to

accumulate and yield an ICCM. This portion of the experiment was termed the “Accumulation” phase. Egressed activity from the donor cells was $\leq 1\%$ of activity added for all concentrations during this phase and activity controls indicated no significant cell death from such activity levels (Boyd *et al.* 2006). Following 1 h, ICCM was removed, passed through a 0.22- μm filter, and added to recipient cells for which the medium had been discarded. These cells were then treated identically to gamma-irradiated cells described above.

A set of cultures was used to determine whether bystander effects were induced in untransfected UVW and EJ138 donor cells undergoing identical [^{131}I]MIBG treatment as described for the NAT gene-transfected cells. NAT-negative cells were labelled “parental”. ICCM from these types was applied to both NAT gene-transfected and untransfected cells.

2.3 Dosimetry Model

When determining the dose to the donor cells used to create the ICCM, dose contributions occurring during both the uptake and accumulation phases of [^{131}I]MIBG treatment need be considered. It is unknown which dose initiates the bystander responses leading to cytotoxic factor accumulation when fresh medium is applied. Previous experiments have illustrated a linear accumulation of MIBG for NAT-expressing cell types during the first two hours of exposure (Armour *et al.* 1994). This coupled with the $\leq 1\%$ egressed activity seen in both UVW/NAT and EJ138/NAT after accumulation (Boyd *et al.* 2006) provides a dose rate function, $\dot{D}(t)$, as illustrated in Figure 1.

Upon application of [^{131}I]MIBG-enhanced medium, the assumption is an instantaneous, homogenous, static mixture uniformly covering all cells with an initial dose rate of \dot{D}_{up} (Gy/h). As donors actively uptake [^{131}I]MIBG over 2 h, dose rate increases linearly up to a maximum dose rate of \dot{D}_{acc} (Gy/h) when the radioactive medium is removed and cells are washed with PBS. When fresh medium is added to allow bystander factors to accrue, the dose rate remains effectively constant at \dot{D}_{acc} due to the negligible amount of egress. Therefore, in order to find the total absorbed dose to the donor cells used to create the ICCM, integration is performed on the function presented in Equation 1 1:

$$D_{\text{tot}} = \frac{\dot{D}_{\text{up}} \cdot \dot{D}_{\text{acc}}}{2}(2\text{h}) + \dot{D}_{\text{acc}}(1\text{h}) \quad (1)$$

where \dot{D}_{up} and \dot{D}_{acc} are the average initial dose rates upon initiation of the uptake and accumulation phases respectively.

To calculate \dot{D}_{up} and \dot{D}_{acc} , the Vynckier-Wambersie point-source dose distribution function (point kernel) is utilized (Vynckier and Wambersie 1982, Vynckier and Wambersie 1986):

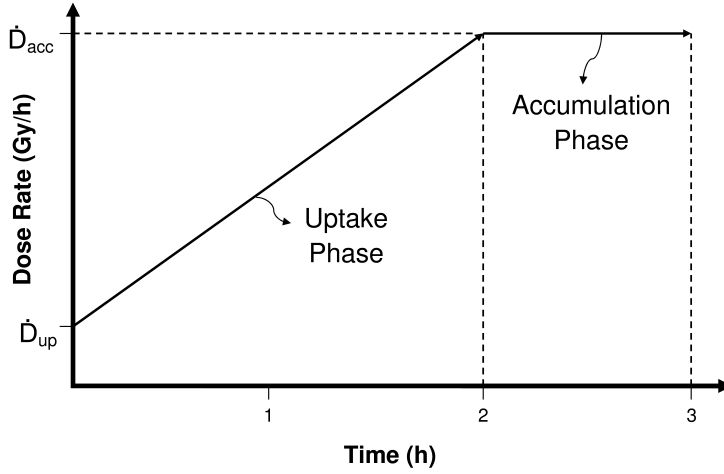


FIGURE 1. Irradiation to donor cells used in the production of irradiated-cell conditioned medium (ICCM) occurs in two phases: i) an uptake phase during which $[^{131}\text{I}]\text{MIBG}$ is taken up by NAT transfected cells and ii) an accumulation phase where fresh medium is applied and bystander factors accrue creating the ICCM. The total dose can be determined through simple integration of the above function.

$$J(x) = \frac{B}{(\rho v x)^2} \left\{ c \left[1 - \frac{\rho v x}{c} e^{\left(1 - \frac{\rho v x}{c}\right)} \right] + \rho v x e^{(1 - \rho v x)} - \rho v x e^{\left(1 - \frac{\rho v x}{2} - \frac{f}{2}\right)} \right\} \quad (2)$$

with $[] \equiv 0$ for $\rho v x \geq c$ and $J(x) \equiv 0$ for $\rho v x \geq f$ where:

$J(x)$ is the absorbed dose rate at a distance x (in cm) from a point source (Gy/MBq·h)

v is an apparent absorption coefficient (in cm^2/g). Within the maximum β -energy range $0.5 \text{ MeV} < E_{\beta_{\max}} < 3.5 \text{ MeV}$, this value can be expressed as a function of $E_{\beta_{\max}}$ (14): $v = 14.5(E_{\beta_{\max}})^{-1.17}$

ρ is the density of the homogenous medium

c is a dimensionless parameter that provides a value for the first term inside the curly brackets to become and remain 0; this parameter was originally defined by Loevinger (Loevinger, Japha and Brownwell, 1956) as:

$$c = \begin{cases} 1 & 1.5 \leq E_{\beta_{\max}} < 3 \text{ MeV} \\ 1.5 & 0.5 \leq E_{\beta_{\max}} < 1.5 \text{ MeV} \\ 2 & 0.17 \leq E_{\beta_{\max}} < 0.5 \text{ MeV} \end{cases}$$

B is a normalization constant evaluated for the requirement that the energy emitted by the point source is equal to the energy absorbed by an infinitely large sphere. It is obtained via:

$$B = (4.6 \times 10^2) \rho^2 v^3 (E_{\beta \text{avg}}) \alpha \text{ in (Gy/MBq} \cdot \text{h)}$$

where

$$\alpha^{-1} = 3c^2 - (c^2 - 1)e + (3 + f)e^{(1-f)} - 4e^{(1-f/2)}$$

and $E_{\beta \text{avg}}$ is the average β -particle energy (in MeV)
 f is a dimensionless parameter where $f/\rho x$ represents the distance at which the β dose is required to be zero. Within the energy range $0.5 \text{ MeV} < E_{\beta \text{max}} < 3.5 \text{ MeV}$, this value can be described as a function of $E_{\beta \text{max}}$ (Vynckier and Wambersie 1986): $f = 0.269 \rho x (E_{\beta \text{max}})^{1.31}$

The Vynckier-Wambersie kernel can be integrated over a number of simple geometries to model a variety of source conditions. Here, two versions of the Vynckier-Wambersie kernel are applied; a) during uptake, a plane of infinite extent and finite thickness and b) during accumulation, a series of planes of infinite extent that are infinitely thin. The Vynckier-Wambersie kernel can be modelled as infinite in extent, with $< 5\%$ correction for radius, provided that the radius of the plane is $\geq 0.5R_{\text{max}}$, the continuous slowing-down approximation (CSDA) range of the most energetic β -particle (The International Commission on Radiation Units and Measurements, 2004). For ^{131}I , $E_{\beta \text{max}}$ is 0.61 MeV resulting in an approximate CSDA maximum range of 0.227 cm. Under these conditions, the Vynckier-Wambersie plane kernel can be modelled with infinite extent down to a surface area covering 0.04 cm². With donor cell treatment occurring in $65\% \pm 5\%$ confluent 25 cm² flasks, the true coverage area is 16.25 cm \pm 1.25 cm. Thus, under these conditions, one can simply apply an identical transformation to all donor flasks, modelling a typical confluent flask as a singular cylindrical slab of cells as illustrated in Figure 2.

As the Vynckier-Wambersie kernel is a function of distance from the source, in order to calculate the dose during both the uptake and accumulation phases, it is required that the thickness of the cells upon adherence to the flask be determined (i.e. determine the thickness of the slab). To accomplish this, it is noted that 2×10^5 cells were plated 24h prior to [¹³¹I]MIBG treatment at which point donor flasks were $65\% \pm 5\%$ confluent in 25 cm² flasks. The cell lines have doubling times of 18 h and 17.5 h for UVW and EJ138 respectively. Thus, the resulting the number of cells present at the time of treatment (C) via:

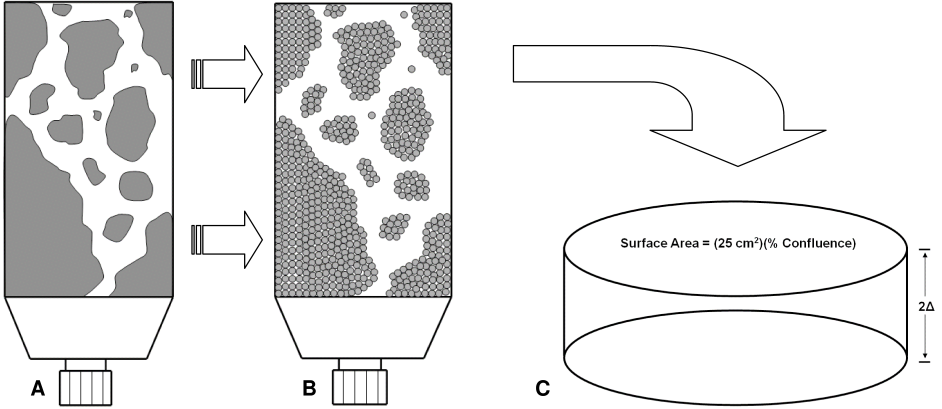


FIGURE 2. Schematic representation of cellular distribution in donor flasks used in irradiated-cell conditioned medium (ICCM). (A) represents an approximation of the actual distribution and (B) represents the same cellular distribution modelled as an aggregation of infinite Vynckier – Wambersie cellular slabs. Since the dose to the entire cellular distribution in (B) is the sum of infinite Vynckier – Wambersie cellular slabs, for simplicity, a single transformation to donor cells is applied in (A) resulting in a single cylindrical slab of cells (C).

$$C = C_0 e^{\frac{(\text{time})\ln 2}{DT}} \quad (3)$$

where C_0 is the number of cells plated and DT is the doubling time of the cell line used. In addition, volume is conserved upon adhesion to the flask relative to the volume of a cell in suspension. Therefore, with knowledge of the diameter of the UVW and EJ138 cell lines ($16.5 \pm 0.9 \mu\text{m}$ and $12.8 \pm 0.7 \mu\text{m}$ respectively), the total volume for the number of donor cells after 24 h (calculated via Eq. 3) in suspension is calculated via:

$$V_{\text{tot}} = C \cdot \left[\frac{4}{3} \pi (0.5 \cdot \text{Cell}_{\text{diam}})^3 \right] \quad (4)$$

and determine the thickness of the cellular slab via:

$$\text{thickness} = 2\Delta = \frac{V_{\text{tot}}}{(\text{Total Flask Growth Surface Area} \cdot \% \text{ Confluence @ treatment})} \quad (5)$$

where Δ is the half thickness of the cellular slab. Given the experimental conditions in (Boyd *et al.* 2006), the resultant cellular slab thickness was calculated as

$$(7.3 \pm 0.9) \times 10^{-5} \text{ cm for UVW and } (3.5 \pm 0.4) \times 10^{-5} \text{ cm for EJ138.}$$

2.4 Dose Rate Calculation: Uptake Phase

As per Figure 1 and Eq. 1, the aim is to calculate the initial dose rate, \dot{D}_{up} , upon application of radiopharmaceutical-enhanced medium to donor cells. This scenario is illustrated in Figure 3.

During donor treatment with $[^{131}\text{I}]\text{MIBG}$, radiopharmaceutical was added to 1 ml of fresh medium during the 2 h allotted for uptake. First, observe that the thickness of this 1 ml of radioactive medium at a density equivalent to water (i.e. 1 g/cm^3) covering a 25 cm^2 growth area results is simply 0.04 cm. The density of the radioactive medium and cellular slab is equivalent. The dose rate at a given distance, x , from our source is dependent on the extent (i.e. diameter), d , of the source as well as its thickness, h , resulting in the function $\dot{D}_{up}(x, h, d)$. From (Vynckier and Wambersie 1986), a source of infinite extent and thickness, h , greater than the maximum range of the most energetic β -particle, the dose rate (in Gy/h) is given by:

$$\dot{D}(x, \infty, \infty) = \dot{D}(0, \infty, \infty) \cdot \alpha \cdot \left\{ c^2 \left[3 - e^{(1-\rho vx)} - \frac{\rho vx}{c} \left(2 + \ln \left(\frac{c}{\rho vx} \right) \right) \right] + e^{(1-\rho vx)} - 4e^{\left(\frac{1-\rho vx}{2} \cdot \frac{f}{2} \right)} + (3 + f - \rho vx)e^{(1-f)} \right\} \quad (6)$$

with $[] \equiv 0$ for $\rho vx \geq c$ and $\dot{D}(x, \infty, \infty) \equiv 0$ for $\rho vx \geq f$.

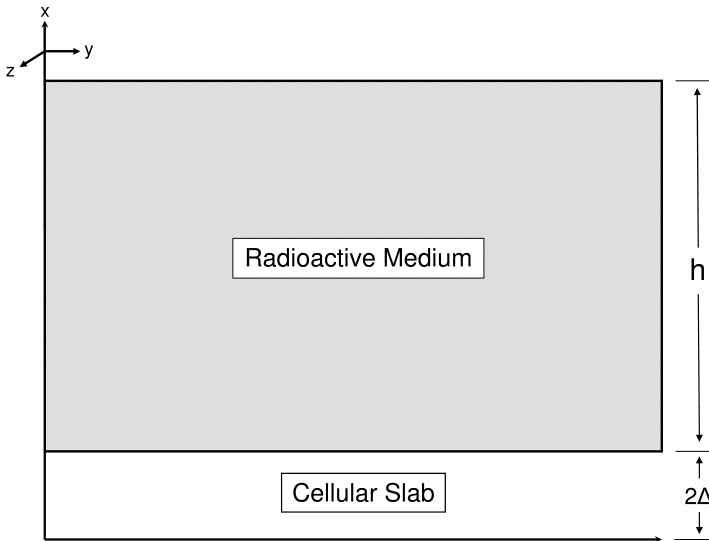


FIGURE 3. Illustration of cell and medium distribution at the onset of the uptake phase immediately following application of radiopharmaceutical.

Additionally, it is noted that $\dot{D}(0,\infty,\infty)$ represents the dose rate (in Gy/h) at the edge of an infinite medium. This is equivalent to the dose rate of a semi-infinite medium or half the dose rate of an infinite medium and is expressed by:

$$\dot{D}(0,\infty,\infty) = 0.288a_m E_{\beta\text{avg}} \quad (7)$$

where a_m is the mass activity concentration (MBq/g) and the average β -particle energy in MeV. In our scenario, with our source of unit density, the value for activity is simply the activity concentration (in MBq/ml = MBq/g = MBq/cm³) administered divided by the number of millilitres of medium (in our case 1 ml). Additionally, since it is assumed that an instant, homogenous, static mixture upon application, radioactive medium covering growth area with no cell present does not contribute dose to the donor cells as this space is effectively located at “infinity”. Therefore, one can adjust for cellular confluence levels and perform a simple modification to Eq. 7 as follows:

$$\dot{D}(0,\infty,\infty) = 0.288(A_{\text{conc_up}})E_{\beta\text{avg}} \quad (8)$$

where $A_{\text{conc_up}} = (A_{\text{admin}})(\% \text{ Confluence})$

With ¹³¹I having a maximum CSDA range of 0.226 cm, five times greater than the thickness of the 1 ml of radioactive medium, the thickness of the source cannot be neglected. From simple geometric considerations, it is determined that (Vynckier and Wambersie 1986):

$$\dot{D}_{\text{up}}(x,h,d) = \dot{D}(x,\infty,\infty) - \dot{D}(x+h,\infty,\infty) \quad (9)$$

Utilizing Eq. 6, 8, and 9, \dot{D}_{up} was calculated at $x = 0$ and 2Δ for $h = 0.04$ cm. The results were averaged to determine the mean dose rate to the slab upon initial application of the [¹³¹I]MIBG-enhanced medium:

$$\dot{D}_{\text{up}} = \left\{ \left[\dot{D}(0,\infty,\infty) - \dot{D}(0.04,\infty,\infty) \right] + \left[\dot{D}(2\Delta,\infty,\infty) - \dot{D}(2\Delta+0.04,\infty,\infty) \right] \right\} / 2 \quad (10)$$

Due to the small magnitude of the cellular slab thickness, there was < 2% difference in $\dot{D}_{\text{up}}(0,0.04,\infty)$ and $\dot{D}_{\text{up}}(2\Delta,0.04,\infty)$ resulting in a < 1% difference between the calculated mean \dot{D}_{up} value and the dose rate at any cellular distance from the source.

2.5 Dose Rate Calculation: Accumulation Phase

Two separate models were developed for comparison and computational efficiency evaluation. The fundamental difference between the models lies in the manner in which the source is distributed within the slab; homogeneously or in discrete planes.

Method #1: “Homogenous-Slab”

During the 1 h accumulation phase, while bystander factors are allowed to accrue in 5 ml of fresh medium, it is assumed that the [¹³¹I]MIBG taken up by the cells is homogeneously distributed within the cellular slab with an activity concentration, $A_{\text{conc_acc}}$ (in MBq/cm³). $A_{\text{conc_acc}}$ is dependent on several factors including cellular confluence, (for analogous reasoning as in the uptake phase), radiopharmaceutical uptake percentage for the cell line, as well as the volume of the cellular slab:

$$A_{\text{conc_acc}} = \frac{(A_{\text{conc_up}})(\% \text{ Uptake})}{(25 \text{ cm}^2)(\% \text{ Confluence})(2\Delta)} \quad (11)$$

The source is split into a bunch of infinitely thin planes of infinite extent with surface activity, A_s , given by $A_{\text{conc_acc}} dx'$ (in MBq/cm²) (see Figure 4). The dose rate contribution from a single plane is $d\dot{D} = A_{\text{conc_acc}} K(x-x',0,\infty) dx'$ where $K(x-x',0,\infty)$ is the Vynckier–Wambersie dose rate kernel for an infinitely thin, infinite extent plane. This expression is given by (Vynckier and Wambersie 1986, The International Commission on Radiation Units and Measurements 2004):

$$K(x-x',0,\infty) = 0.288 \cdot v \cdot \alpha \left\{ c \left[1 + \ln \left(\frac{\rho v(x-x')}{c} \right) - e^{\left(1 - \frac{\rho v(x-x')}{c} \right)} \right] + e^{(1-\rho v(x-x'))} - 2e^{\left(1 - \frac{\rho v(x-x')}{c} - \frac{f}{2} \right)} + e^{(1-f)} \right\} \quad (12)$$

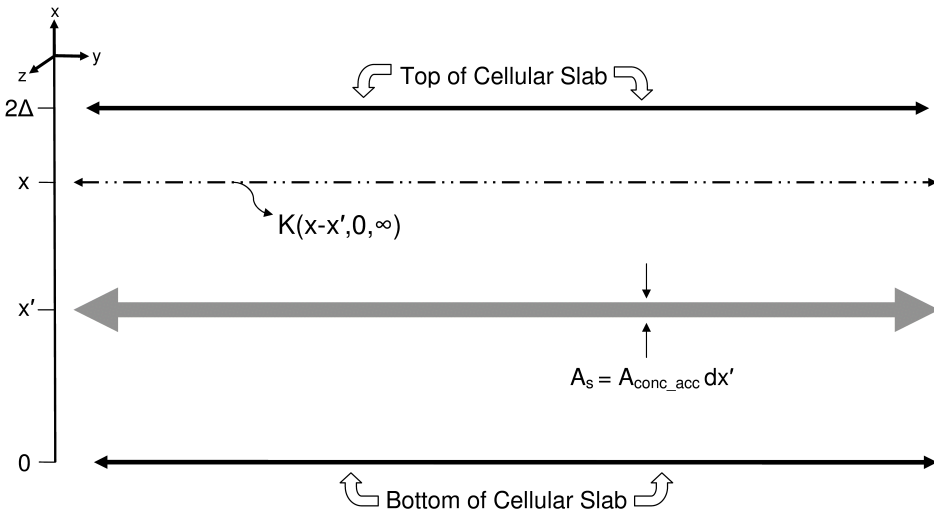


FIGURE 4. Illustration of Method #1 radiopharmaceutical modelling during the accumulation phase. The source is considered split into a bunch of infinite thin disks of surface activity $A_s = A_{\text{conc_acc}} dx'$ (MBq/cm²). For a point x a distance $x-x'$ from the source, the dose rate contribution is given by $d\dot{D} = A_{\text{conc_acc}} K(x-x',0,\infty) dx'$ where $K(x-x',0,\infty)$ is the Vynckier–Wambersie dose rate kernel for a plane that is infinitely thin and of infinite extent.

To determine the expression for the total dose rate to the cellular slab during the accumulation, integrate over the range $x = 0$ to 2Δ :

$$\dot{D}(x) = A_{\text{conc_acc}} \int_{x'=0}^{x'-2\Delta} \dot{K}(x-x', 0, \infty) dx' \quad (13)$$

The kernel is actually a function of the distance from the plane to the point of measurement (i.e. $|x-x'|$). To compensate for this, a change of variables to $u = x-x'$ is made resulting in:

$$\dot{D}(x) = A_{\text{conc_acc}} \left[\int_{x-2\Delta}^0 \dot{K}(u, 0, \infty) du + \int_0^x \dot{K}(u, 0, \infty) du \right] \quad (14)$$

Then, let $u = |v|$ providing:

$$\dot{D}(x) = A_{\text{conc_acc}} \left[\int_0^{2\Delta-x} \dot{K}(v, 0, \infty) dv + \int_0^x \dot{K}(v, 0, \infty) dv \right] \quad (15)$$

Lastly, the average dose rate to the slab, \dot{D}_{acc} , is obtained by determining the average dose rate from Eq. 13 over the entire thickness of the slab:

$$\dot{D}_{\text{acc}} = \frac{1}{2\Delta} \int_0^{2\Delta} \dot{D}(x) dx \quad (16)$$

Method #2: “Multi-isoplane”

Due to the relative thinness of the cells upon adherence to the culture flasks, a second model was created with the aim of improving on the computational efficiency of the model calculations during the accumulation phase while maintaining the same degree of precision as Method #1. To do this, two paradigms were created in which the activity was evenly distributed into isolated, homogenous planes and dose rates were computed at various positions within the slab (see Figure 5). Paradigm (A) calculates the dose rate at positions $x = 0, \Delta,$ and 2Δ with source planes at $x = 0.5\Delta$ and 1.5Δ while paradigm (B) calculates the dose rate at $x = 0.5\Delta$ and 1.5Δ with source planes at positions $x = 0, \Delta,$ and 2Δ . The surface activity of given plane is provided by:

$$\begin{aligned} A_{\text{tot_acc}} &= \frac{1}{2} A_{\text{surf_acc}} + \frac{1}{2} A_{\text{surf_acc}} \quad \text{for Paradigm (A)} \\ &= \frac{1}{3} A_{\text{surf_acc}} + \frac{1}{3} A_{\text{surf_acc}} + \frac{1}{3} A_{\text{surf_acc}} \quad \text{for Paradigm (B)} \end{aligned} \quad (17)$$

with,

$$A_{\text{surf_acc}} = \frac{(A_{\text{conc_up}})(\% \text{ Uptake})}{(25 \text{ cm}^2)(\% \text{ Confluence})} \quad (18)$$

The dose rate at a various positions x_{1-5} are given by:

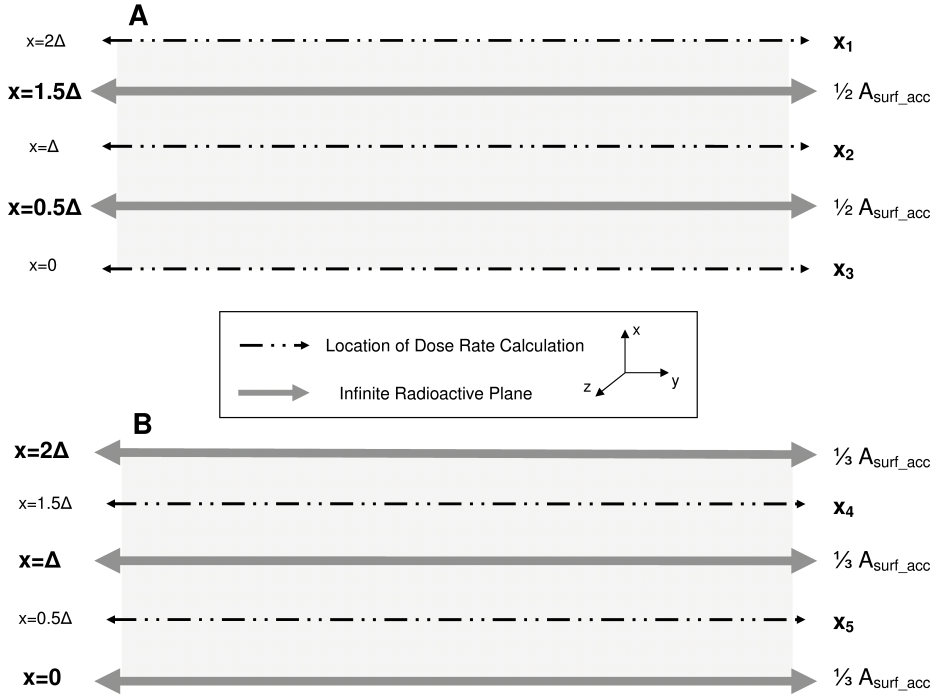


FIGURE 5. Illustration of Method #2 radiopharmaceutical modelling during the accumulation phase. The dose rate along five separate planes is calculated via one of two paradigms: (A) For equally distributed activity in two infinite planes located at $x = 0.5\Delta$ and 1.5Δ , calculate \dot{D} at $x = 0, \Delta$, and 2Δ (Paradigm #1). (B) For equally distributed activity in three infinite planes located at $x = 0, \Delta$, and 2Δ , calculate \dot{D} at $x = 0.5\Delta$ and 1.5Δ . The average dose rate to the slab, \dot{D}_{acc} , is calculated as the average dose rate from these five locations.

$$\dot{D}(x_1) = \left(\frac{1}{2} A_{surf_acc}\right)K(1.5\Delta, 0, \infty) + \left(\frac{1}{2} A_{surf_acc}\right)K(0.5\Delta, 0, \infty) = \dot{D}(x_3) \quad (19)$$

$$\dot{D}(x_2) = 2 \cdot \left(\frac{1}{2} A_{surf_acc}\right)K(0.5\Delta, 0, \infty) \quad (20)$$

$$\dot{D}(x_4) = 2 \cdot \left(\frac{1}{3} A_{surf_acc}\right)K(0.5\Delta, 0, \infty) + \left(\frac{1}{3} A_{surf_acc}\right)K(1.5\Delta, 0, \infty) = \dot{D}(x_5) \quad (21)$$

The final dose rate during the accumulation phase using Method #2 is:

$$\dot{D}_{acc} = \frac{1}{5} \sum_{i=1}^5 \dot{D}(x_i) \quad (22)$$

The results of Eq. 10 and either 16 or 22 were substituted into Eq. 1 in order to obtain the total dose to the donor cells used to create the ICCM for recipient cell treatment.

2.6 Software and Statistics

All modelling and calculations were performed using MATLAB 7.9.0 (R2009b; 32-bit; The Mathworks). Analytical integration for the “homogenous-slab” model was performed leveraging either the MATLAB Symbolic Toolbox (ver. 5.3) MuPAD engine or the Maple 13 (Maplesoft) symbolic engine. Two separate MATLAB M-file programs were created: a) comparing the “homogenous-slab” and “multi-isoplane” models during accumulation phase for dose rate results and computation time; and b) the complete dosimetry model allowing automatic calculation of cell slab thickness, dose rates during uptake and accumulation phases (using “multi-isoplane” model), and total ICCM dose following user input of the various experimental parameters outlined in Boyd *et al.*’s original work (Boyd *et al.* 2006). Both of these programs can be run within the MATLAB environment with output for the dosimetry model being directed to either the terminal or a variety of Microsoft Excel file formats. In addition to this, a standalone Microsoft Windows operating system (OS) application was created for the dosimetry model via utilization of MATLAB’s ‘deploytool’ package and MATLAB compiler (ver. 4.11). This standalone executable was developed to run on any Windows-based host OS, independent of any MATLAB installation, after a one-time installation of the MATLAB Compiler Runtime libraries (ver. 7.11) delivered with the executable. This application was tested successfully under Windows XP (NT 5.1; SP 3; 32-bit) and Windows 7 (NT 6.1; SP 1; 64-bit) operating systems. All modelling and calculations were performed on the same machine containing an Intel Core 2 Duo T5870 processor at 2.00 GHz (L1 cache = 64 KB; L2 cache = 2 MB) with 3.0 GB of RAM (SODIMM DDR2 at 667 MHz) running a Windows 7 (SP 1) OS.

Particle range data was obtained through the ESTAR program developed by the National Institute of Standards and Technology (NIST) Physical Measurement Laboratory utilizing water as the medium. Recipient cell surviving fractions is presented as the mean \pm standard deviation (SD) with significance determined via student’s *t* test with confidence value $p = 0.05$. Uncertainty in dose was determined through traditional propagation uncertainty methods (i.e. “square root of the sum of squares”) from mean \pm minimum/maximum dose rate values obtained from optimization of values for cell slab thickness, donor flask confluence, and [¹³¹I]MIBG uptake percentage (e.g. maximum dose rate during the accumulation phase for Method #1 occurs for maximum uptake percentage for the smallest slab thickness and donor flask confluence).

3. RESULTS

Comparison of dose rate values and computational performance between “homogenous-slab” and “multi-isoplane” modelling of dose rate during accumulation phase

As an approximated method had been developed (“multi-isoplane” source; Method #2) to model the dose rate to donor cells during ICCM production (“Accumulation Phase”), comparison of the dose rate calculations versus the “homogenous-slab” source (Method #1) was undertaken in order to determine the optimal methodology to employ. It was anticipated that both methods would yield answers that were in agreement and the method that produced the least amount of computational overhead would be utilized. For an activity concentration of 1 MBq/ml and experimental parameters associated with UVW/NAT donor cells, the average dose rate results for each method as well as computation time required are shown in Table 1.

As would be expected, both MATLAB’s inherent MuPAD symbolic engine and Maple’s symbolic engine yielded identical dose rate results via the “homogenous-slab source” model. The Maple symbolic engine greatly outperformed MuPAD in computational efficiency by performing the identical calculation over 7 times faster. By comparison, our “multi-isoplane” model yielded an answer well within agreement of the Method #1 answer, with equivalent relative uncertainty. In addition, this method was over 185 times more efficient than even Maple’s symbolic engine. These results directed the use of the “multi-isoplane” method in the further examination of complete survival fraction data from (Boyd *et al.* 2006).

Calculation of dose for [¹³¹I]MIBG ICCM and corresponding examination of UVW/NAT and EJ138/NAT recipient cell survival curves

Utilizing the “multi-isoplane” method during the ICCM “accumulation” phase coupled with the associated Vynckier-Wambersie derived expression for a finite-thick, β -emitting slab during the uptake phase, dose rates and overall absorbed doses to UVW and EJ138 were calculated.

TABLE 1. Comparison of modelling methodologies used to calculate dose rate during ICCM production.

	Avg. Dose Rate during ICCM production (Gy/h)	Avg. Computation Time per Calculation ^a (s)
Method #1a (MuPAD)	0.0999 \pm (0.033/0.025)	30.84 \pm 0.41
Method #1b (Maple)	0.0999 \pm (0.033/0.025)	3.98 \pm 0.54
Method #2	0.0937 \pm (0.031/0.024)	0.0215 \pm 0.0021

^a Calculations measured over 9 independent trials (n = 9) after memory cleared and represented as total time to calculate dose rate and uncertainties \pm SD.

First, the cellular slab thickness was determined for each cell line, resulting in values of $0.73 \mu\text{m} \pm 0.09 \mu\text{m}$ for UVW and $0.35 \mu\text{m} \pm 0.04 \mu\text{m}$ for EJ138. Next, activity concentrations of [^{131}I]MIBG ranging from 1-8 MBq/ml and 1 - 11 MBq/ml for UVW and EJ138 respectively were utilized to calculate the dose rate during both phases. Mean dose rates ranged from 0.015 to 0.116 Gy/h for UVW and 0.014 to 0.161 Gy/h for EJ138 during the uptake phase. Corresponding absorbed dose values to parental cell lines (i.e. not transfected with NAT resulting in no active MIBG uptake and no resulting accumulation phase) are presented for UVW and EJ138 in Figure 6. As clearly seen, the mean dose received by these donor lines is relatively small, obtaining a maximum of only 0.23 Gy for UVW and 0.32 Gy for EJ138 parental lines.

By contrast, dose rate at the initiation of the accumulation phase was significantly greater through the entire spread of activity calculations applied. For UVW/NAT cells, mean dose rates ranged from 0.09 to 0.75 Gy/h while EJ138/NAT mean dose rates ranged from 0.07 to 0.78 Gy/h for the respective range of activity concentrations examined. Total dose to the donor cells producing the ICCM was calculated using Eq. 1 and recipient survival fraction data was plotted for both transfected cell lines (Figure 7; bottom x-axis). For comparison purposes, ^{60}Co data for these cell lines (Boyd *et al.* 2006) is also shown (Figure 7; top x-axis).

Both UVW/NAT and EJ138/NAT require a relatively small ICCM treatment dose to yield a substantial bystander response in recipient cells

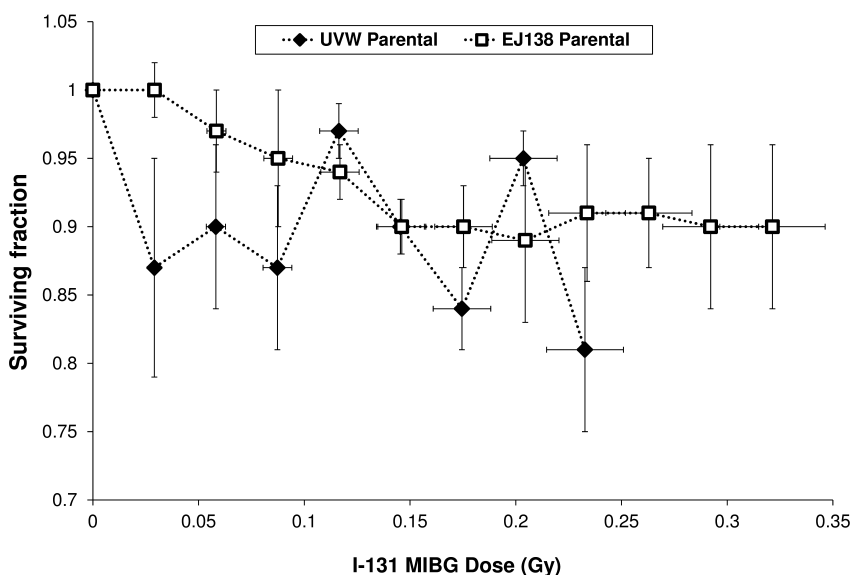


FIGURE 6. Plot of recipient surviving fraction (SF) data following ICCM treatment for UVW and EJ138 Parental donor cell types. All SF data was collected across 6 independent experiments performed in triplicate and represented as mean \pm SD (Boyd *et al.* 2006).

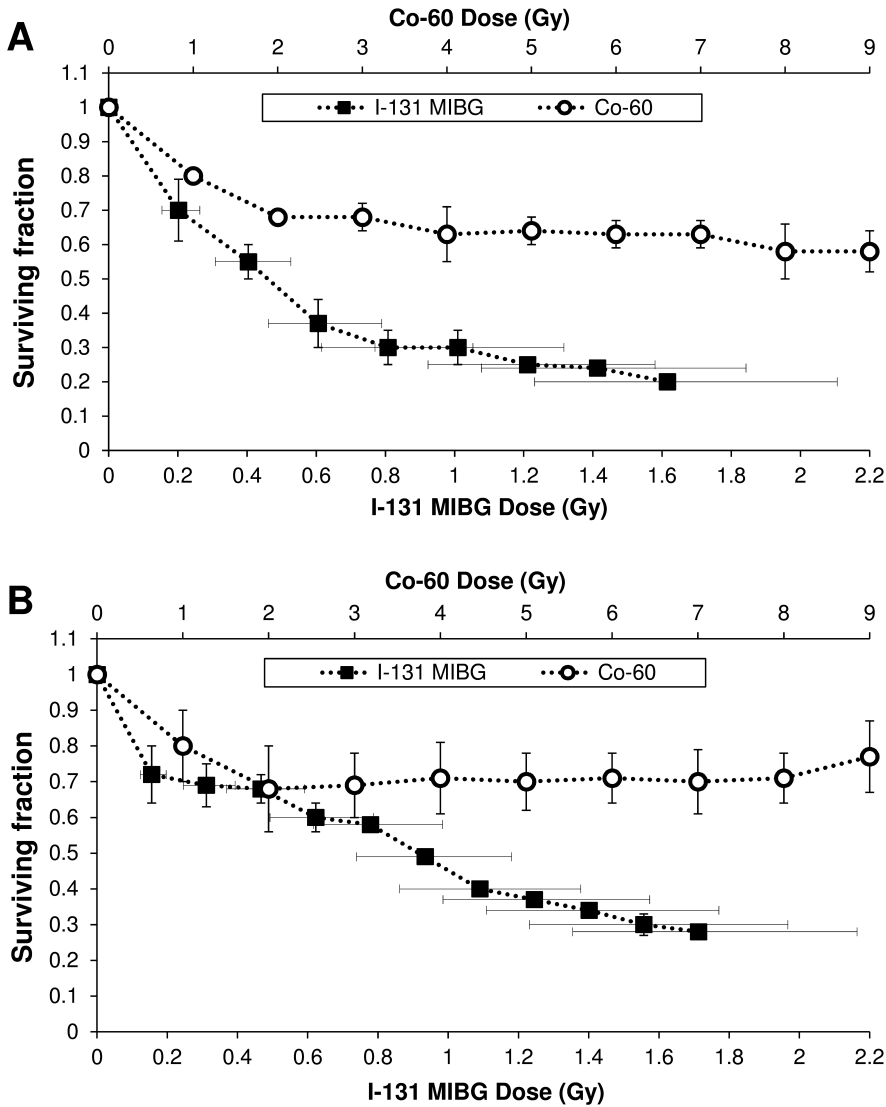


FIGURE 7. Plot of surviving fraction (SF) data for (A) UVW/NAT and (B) EJ138/NAT recipient cells treated with ICCM from either ^{131}I MIBG or ^{60}Co irradiation. All SF data was collected across 6 independent experiments performed in triplicate and represented as mean \pm SD (Boyd *et al.* 2006).

compared to that used in ^{60}Co treatment. An initial activity concentration of 1 MBq/ml yields mean dose to donor cells of 0.2 and 0.15 Gy for UVW/NAT and EJ138/NAT, increasing with activity concentration and yielding a maximum mean dose 1.6 and 1.7 Gy for each cell line respectively. It is also evident that both cell lines show a decrease in the rate of bystander cell death as dose increases and approaches 2 Gy.

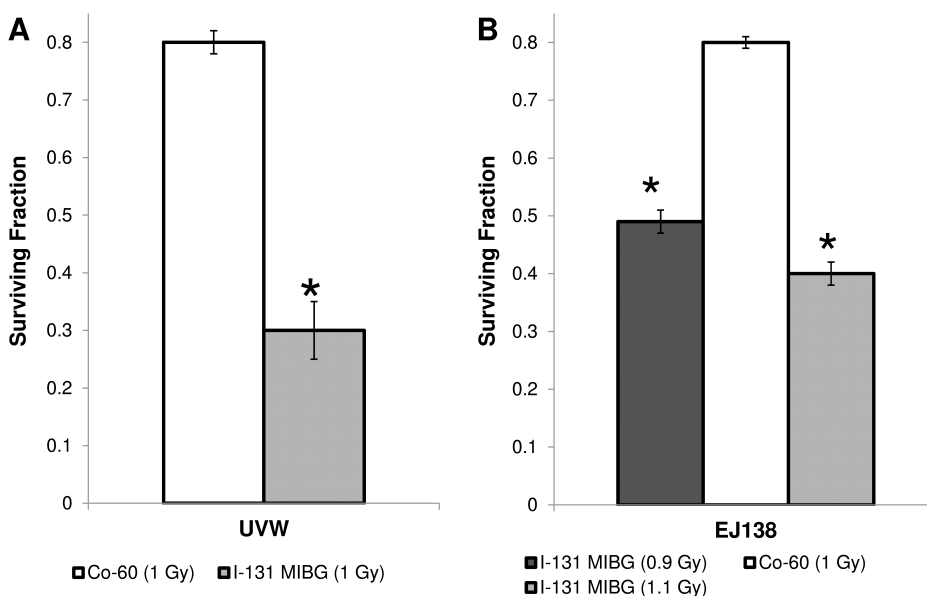


FIGURE 8. Comparison of surviving fraction (SF) of (A) UVW/NAT and (B) EJ138/NAT [¹³¹I]MIBG data with similar ⁶⁰Co dose end points. All SF data was collected across 6 independent experiments performed in triplicate and represented as mean ± SD. * indicates p < 0.05 for difference in SF at the same dose point.

Comparison of survival fractions for identical mean dose ICCM treatments from ⁶⁰Co and [¹³¹I]MIBG

Lastly, surviving fractions of identical or nearly identical mean dose points were examined between ⁶⁰Co (at a dose rate of 15 Gy/h) and [¹³¹I]MIBG ICCM treatments. Figure 8 provides the comparison of these ICCM treatments for UVW/NAT (A) and EJ138/NAT (B). Both cell lines appear to have very similar behaviour compared to their ⁶⁰Co treated counterpart. For UVW/NAT cells, 5 MBq/ml [¹³¹I]MIBG treatment provided a 50% increase bystander cell death efficiency at a mean maximum dose rate during the accumulation phase of 0.47 Gy/h. On the other hand, EJ138/NAT cells provided a 31% to 40% increase in efficiency at dose points within 10% of 1 Gy ⁶⁰Co treatment at mean maximum dose rates ranging from 0.42 Gy/h to 0.49 Gy/h.

4. DISCUSSION

Targeted radionuclide therapy seeks to deliver cytotoxic doses of radiation to malignant foci. This can be confounded by several factors, including heterogeneous uptake of radiopharmaceutical. Non-uniform dose distribution may be overcome, through the use of long-range β-emitters by exploiting the physical bystander effect, which results from

signalling between irradiated and neighbouring non-irradiated cells. Furthermore, toxicity to untargeted regions of tumors may result from the production of cytotoxic factors from cells which accumulate radiopharmaceutical (Boyd *et al.* 2006). This effect has been described in a variety of systems over the last 20 years indicating the existence of RIBBEs both *in vitro* and *in vivo* (Brooks 2004). Such effects are reported following both of high – and low – LET irradiations and have been cited as possibly dependent on a number of factors including cytokine release (Gow *et al.* 2010), nitric oxide (Shao *et al.* 2008), gap – junction communication (Shao *et al.* 2003), and reactive oxygen species (ROS) / free radical formation (Azzam *et al.* 2002).

A limitation of radiopharmaceutical RIBBE experiments presented so far has been the lack of ability to determine appropriate absorbed dose levels to donor cells resulting from radiopharmaceutical treatment utilized to create ICCM. As a consequence, recipient surviving fraction, typically measured against absorbed donor dose, has been compared with administered radiopharmaceutical activity concentration. This does not enable a comparative evaluation of internalised radionuclides and external beam radiation with respect to their induction of bystander effects. Therefore, the goal of the current study was to develop a method to calculate absorbed dose to donor cells used in ICCM production following [¹³¹I]MIBG treatment.

One of the first challenges in this study was an accurate and efficient means to model the source distribution after radiopharmaceutical uptake. This led to the development of both “homogenous-slab” and “multi-isoplane” source distributions during the accumulation phase. The hypothesis was that due to the relatively thinness of the cells adhering to the surface of a culture flask, the “multi-isoplane” model would provide equivalent calculations for dose rates while being computational more efficient than the “homogenous-slab” model regardless of symbolic engine. The data presented in Table 1 confirms the success of this approach with orders of magnitude in computational efficiency achieved. Furthermore, the code structure for implementation of the “multi-isoplane” model into the overall absorbed dose calculation model allowed it to be compiled via the MATLAB C-Compiler (mcc) something not possible through utilization of the MuPAD or Maple symbolic engine. This allowed for creation of a standalone, Windows – based application that can be utilized for future experiments without the need for acquisition or personal knowledge of the MATLAB environment. This code base can also be shared and modified allowing for additional enhancements and dosimetry modelling within the wider scientific community.

The first surviving fraction behaviour examined was that of the parental cell lines of UVW and EJ138. In the absence of active uptake of [¹³¹I]MIBG, it was anticipated that a smaller dose and dose rate would

result during the uptake phase explaining the lack of bystander cell death observed. The corresponding calculated dose to the parental cell lines fits this hypothesis achieving only maximal mean doses of 0.23 and 0.32 Gy for UVW and EJ138 respectively. Even for cell lines whose bystander effects have been characterized, typical survival fraction drops are relatively small (10-15% from control) using medium transfer protocols for doses of 0.5 Gy (Ryan *et al.* 2008, Gow *et al.* 2008). Thus, the findings support the predictions of the dosimetry model developed.

Next, absorbed dose values for [¹³¹I]MIBG treatments for transfected UVW/NAT and EJ138/NAT donor cells were examined and compared with dose delivered by external beam (Figure 7). It was observed that the rate of bystander cell death decreased as dose increased. Absorbed dose calculations for [¹³¹I]MIBG treatment indicate that ICCM production never resulted in a cell killing plateau as seen after 2 Gy with external beam treatment. However, in response to [¹³¹I]MIBG treatment, there was a trend toward a plateau with respect to clonogenic cell kill as treatment dose approached 2 Gy. This finding again supports the validity of the dosimetry model implemented as similar overall behaviour of the surviving fraction curve would be expected for the same cell lines and for similar low – LET irradiation and dose values.

While similar trends are apparent in surviving fraction curve behaviour, significant differences are also obvious in the magnitude of the bystander cell death response following [¹³¹I]MIBG versus external beam treatment (Figure 8). Two essential differences in treatment are: (a) radiation type (β – particles versus γ – rays) and (b) dose rate (UVW were subjected to 0.09 Gy/h – 0.75 Gy/h and EJ138 were subjected to 0.07 Gy/h – 0.78 Gy/h in the form of [¹³¹I]MIBG treatment whereas external beam radiation was delivered at 15 Gy/h). With respect to radiation type, it has long been recognized in experimental biology that similar LET radiations do not all have the same effectiveness at inducing cellular damage. Using human lymphocytes and mouse oocytes, it has been shown that 200 kV x – rays are two – three times as effective as γ – rays at inducing chromosome aberrations (Bond *et al.* 1978, Edwards *et al.* 1982) while ⁶⁰Co γ – rays have been shown to be three times more effective than 15 MeV electrons utilizing the same end point (Edwards *et al.* 1982). Experiments by Sasaki *et al.* (1989) and Schmid *et al.* (2002) have also pointed to a higher rate of chromosome aberrations by lower LET x – rays relative to high energy γ – rays. Furthermore, for bystander responses in particular, our group has indicated a significant difference in bystander cell death by ⁶⁰Co γ – rays compared with 20 MeV electrons for low, nearly equivalent, clinical dose rate at high doses (Gow, 2008). Therefore, radiation type cannot be neglected as potentially playing a role in the observed differences in bystander cell death.

Low dose rate (LDR) irradiation (0.1 Gy/h to 1 Gy/h) has been reported to affect multiple biological processes in both normal and tumour cell types (Gridley *et al.* 2005) and been discussed as potentially relevant for radionuclide therapy (Sgouros *et al.* 2007). Decreases in dose rate are often associated with sparing effects of direct irradiation (Hall and Bedford 1964) but have been also shown to invoke a hypersensitivity in some cell lines leading to an increase in cell death relative to higher dose rates (i.e. 'inverse dose-rate effect') (Mitchell *et al.* 2002). These inverse dose-rate effects have been observed in a variety of cell types (DeWeese *et al.* 1998, Mitchell *et al.* 2002, Widel and Przybyszewski 1998) and have been postulated as to reflect the hyper-radiosensitivity of cell lines in responses to a small, acute dose (Mitchell *et al.* 2002). Animal studies have also illustrated the effectiveness of ^{131}I labelled antibody treatment and low-dose rate versus high-dose rate exposure in significantly decreasing tumour volume (Knox *et al.* 1990). While the precise mechanisms underlying LDR effects are not completely defined, they are clearly complex. Any correlation between LDR and bystander effects is currently unclear but we cannot exclude the possibility that direct LDR effects would influence subsequent bystander responses measurable through the medium transfer protocol. In fact, the evidence presented here suggests that low dose rates may be a dominant contributing factor to the observed biological bystander cell death.

Although not directly examined here, the bystander responses seen in ICCM production with [^{123}I] MIBG and [^{211}At] MABG, high LET radiopharmaceuticals are discussed in Boyd *et al.* (2006). These results indicate in both cases that a maximum bystander response is reached followed by a substantial decrease in bystander response resulting in a distinct U – shaped surviving fraction curve. This phenomenon has also been seen by our group in normal HPV-G keratinocytes (Gow *et al.* 2008) and in malignant T98G glioma (Gow *et al.* 2010). In both the conventional and targeted protocols, the reduction of bystander signal strength to near control levels following lower dose induced production of significant bystander cell death was observed. We suggest that in the case of radiopharmaceuticals, several contributing factors could be involved including high LET, relatively short particle range, and extranuclear cell accumulation of these radiopharmaceuticals. Dosimetry models for [^{123}I] MIBG and [^{211}At] MABG may yield high absorbed dose values at the top end activity concentrations tested. This offers a plausible explanation for the observed U – shaped behaviour and is a potential area for further investigation.

Another point of interest involves whether this model is adaptable or not for targeted high-LET radiotherapy. To do this would require an adequate dose point kernel (DPK) flexible enough to model via similar geometries and take into account differing radiation parameters (ex.

path length and approximating “infinite” sources). Additionally, the structure of the DPK may limit utilization of computational efficiencies created via the multi-isoplane approximation. As such, integrating a high-LET DPK into our code base, should an adequate model exist today, is possible and could theoretically extend our results under appropriate circumstance. Otherwise, more complex mathematical modeling would be required.

5. CONCLUSION

In this study, a computationally efficient model for determining absorbed dose values following β -emitting radiopharmaceutical treatment was developed. This model was applied to experimental protocol outlined by Boyd *et al.* (2006) and used to provide direct comparison with gamma radiation from an external beam source. This dosimetry provides a plausible, quantitative explanation for the absence of a bystander response in cells which were incapable of active accumulation of radiopharmaceutical. An explanation is also provided for the overall behaviour and shape of surviving fraction curves for NAT transfected recipients capable of active radiopharmaceutical uptake. The model points to the possibility of LDR effects as an explanation for the observed increase in efficiency of bystander cell kill following [¹³¹I]MIBG treatment. Through development of a standalone application for the dosimetry model, further investigation of bystander responses induced by targeted radiopharmaceuticals has been made possible. Identification of RIBBE factors will aid in the development of novel targeted radiopharmaceutical treatment, maximizing malignant cell death and sparing normal tissue.

ACKNOWLEDGEMENTS

The authors would like to mention and give thanks Andrei Hanu and Jennifer Fazzari (McMaster University) for their MATLAB insights in the early stages of this endeavour and editing respectively.

REFERENCES

- Armour A, Mairs R J, Gaze M N, and Wheldon T E 1994 Modification of meta-iodobenzylguanidine uptake in neuroblastoma cells by elevated temperature Br.J.Cancer. 70 445-448
- Azzam E I, de Toledo S M, Spitz D R, and Little J B 2002 Oxidative metabolism modulates signal transduction and micronucleus formation in bystander cells from alpha-particle-irradiated normal human fibroblast cultures Cancer Res. 62 5436-5442
- Bond V P, Meinhold C B, and Rossi H H 1978 Low-dose RBE and Q for x-ray compared to gamma-ray radiations Health Phys. 34 433-438
- Boyd M, Cunningham S H, Brown M M, Mairs R J, and Wheldon T E 1999 Noradrenaline transporter gene transfer for radiation cell kill by ¹³¹I meta-iodobenzylguanidine Gene Ther. 6 1147-1152
- Boyd M, Mairs R J, Keith W N, Ross SC, Welsh P, Akabani G, Owens J, Vaidyanathan G, Carruthers R, Dorrens J, and Zalutsky MR 2004 An efficient targeted radiotherapy/gene therapy strategy utilising human telomerase promoters and radioastatine and harnessing radiation-mediated bystander effects. J. Gene. Med. 6 937-947

- Boyd M, Ross S C, Dorrens J, Fullerton NE, Tan KW, Zalutsky MR, and Mairs RJ. 2006 Radiation-induced biologic bystander effect elicited in vitro by targeted radiopharmaceuticals labeled with alpha-, beta-, and auger electron-emitting radionuclides *J. Nucl. Med.* 47 1007-1015
- Brooks A L 2004 Evidence for 'bystander effects' in vivo *Hum Exp Toxicol.* 23 67-70
- Cunningham S, Boyd M, Brown M M, Carlin S, McCluskey A, Livingstone A, Mairs RJ, and Wheldon TE. *Med Pediatr Oncol.* 2000 A gene therapy approach to enhance the targeted radiotherapy of neuroblastoma. *Med. Pediatr. Oncol.* 35 708-711
- DeWeese T L, Shipman J M, Dillehay L E, and Nelson W G 1998 Sensitivity of human prostatic carcinoma cell lines to low dose rate radiation exposure *J. Urol.* 159 591-598
- Edwards A A, Lloyd R J, Purott J S, and Prosser J S, 1982. The dependence of chromosome aberration yields on dose rate and radiation quality. In: *Research and development report 1979 - 1981, RAD 4.* Clinton, UK: National Radiological Protection Board, pp.83.
- Fullerton N E, Mairs R J, Kirk D, Keith W N, Carruthers R, McCluskey A G, Brown M, Wilson L, and Boyd M. 2005 Application of targeted radiotherapy/gene therapy to bladder cancer cell lines *Eur.Urol.* 47 250-256
- Gow M D, Seymour C B, Byun S H, and Mothersill C E 2008 Effect of dose rate on the radiation-induced bystander response *Phys Med Biol.* 53 119-132
- Gow M D, Seymour C B, Ryan L A, and Mothersill C E 2010 Induction of bystander response in human glioma cells using high-energy electrons: a role for TGF-beta1 *Radiat Res.* 173 769-778
- Gridley D S, Williams J R, and Slater J M 2005 Low-dose/low-dose-rate radiation: a feasible strategy for cancer radiotherapy? *Cancer Ther.* 3 105-130
- Hall E J and Bedford J S 1964 Dose Rate: Its Effect on the Survival of HeLa Cells Irradiated with gamma rays *Radiat. Res.* 22 305-315
- The International Commission on Radiation Units and Measurements, 2004. Appendix C: Calculation of Beta-Ray Dose Distributions By Integration of the Beta-Ray Point-Source Dose Function. In: *Dosimetry of Beta Rays and Low-Energy Photons for Brachytherapy with Sealed Sources.* Bethesda, MD: Oxford University Press, pp.155.
- Jacques Jr S, Tobes M C, Sisson J C, Baker J A, and Wieland D M 1984 Comparison of sodium dependence of uptake of meta-iodobenzylguanidine and norepinephrine into cultured bovine adrenomedullary cells *Mol. Pharmacol.* 26 539-546
- Knox S J, Levy R, Miller R A, Uhland W, Schiele J, Ruehl W, Finston R, Day-Lollini P, and Goris M L. 1990 Determinants of the antitumor effect of radiolabeled monoclonal antibodies *Cancer Res.* 50 4935-4940
- Kufe D, and Weichselbaum R 2003 Radiation therapy: activation for gene transcription and the development of genetic radiotherapy-therapeutic strategies in oncology *Cancer Biology Therapy* 63 326-329
- Loevinger R, Japha E M, and Brownwell G L 1956. *Discrete radioisotope sources. I. Beta-radiation.* New York: Academic Press, pp.694.
- Mairs RJ, and Boyd M 2003 Targeting Radiotherapy to Cancer by Gene Transfer. *J. Biomed. Biotechnol.* 102-109.
- Mairs R J, and Boyd M 2008 Optimizing MIBG therapy of neuroendocrine tumors: preclinical evidence of dose maximization and synergy *Nucl. Med. Biol.* 35 Suppl 1 S9-20
- Mairs R J, Russell J, Cunningham S, O'Donoghue J A, Gaze M N, Owens J, Vaidyanathan G, Zalutsky MR. 1995 Enhanced tumour uptake and in vitro radiotoxicity of no-carrier-added [¹³¹I]meta-iodobenzylguanidine: implications for the targeted radiotherapy of neuroblastoma *Eur.J.Cancer.* 31A 576-581.
- Mairs RJ 1999. Neuroblastoma therapy using radiolabelled [¹³¹I]meta-iodobenzylguanidine ([¹³¹I]MIBG) in combination with other agents *Eur. J. Cancer* 35 1171-1173
- Mitchell C R, Folkard M, and Joiner M C 2002 Effects of exposure to low-dose-rate (60)co gamma rays on human tumor cells in vitro *Radiat. Res.* 158 311-318
- Mitrofanova E, Unfer R, Vahanian N, and Link C 2006 Rat sodium iodide symporter allows using lower dose of ¹³¹I for cancer therapy *Gene Ther.* 13 1052-1056
- Mothersill C, and Seymour C 1997 Medium from irradiated human epithelial cells but not human fibroblasts reduces the clonogenic survival of unirradiated cells *Int J Radiat Biol.* 71 421-427
- Perez C A, and Brady L W. eds., 1998. *Principles and practice of radiation oncology.* Philadelphia, PA: Lippincott-Raven Publications, pp. 957.
- Ryan L A, Smith R W, Seymour C B, and Mothersill C E 2008 Dilution of irradiated cell conditioned medium and the bystander effect *Radiat Res.* 169 188-196

Dose calculations for [¹³¹I]MIBG induced RIBBE

- Sasaki M S, Kobayashi K, Hieda K, Yamada T, Ejima Y, Maezawa H, Furusawa Y, Ito and T, Okada S. 1989 Induction of chromosome aberrations in human lymphocytes by monochromatic X-rays of quantum energy between 4.8 and 14.6 keV *Int. J. Radiat. Biol.* 56 975-988
- Schmid E, Regulla D, Kramer H M, and Harder D 2002 The effect of 29 kV X rays on the dose response of chromosome aberrations in human lymphocytes *Radiat. Res.* 158 771-777
- Sgouros G, Knox S J, Joiner M C, Morgan W F, and Kassis A I 2007 MIRD continuing education: Bystander and low dose-rate effects: are these relevant to radionuclide therapy? *J. Nucl. Med.* 48 1683-1691
- Shao C, Folkard M, and Prise K M 2008 Role of TGF-beta1 and nitric oxide in the bystander response of irradiated glioma cells *Oncogene* 27 434-440
- Shao C, Furusawa Y, Aoki M, and Ando K 2003 Role of gap junctional intercellular communication in radiation-induced bystander effects in human fibroblasts *Radiat Res.* 160 318-323
- Vynckier S, and Wambersie A 1982 Dosimetry of beta sources in radiotherapy I. The beta point source dose function *Phys Med Biol.* 27 1339-1347
- Vynckier S, and Wambersie A 1986 Dosimetry of beta sources in radiotherapy: Absorbed dose distributions around plane sources *Radiation Protection Dosimetry* 14 169-173
- Widel M, and Przybyszewski W M 1998 Inverse dose-rate effect for the induction of micronuclei in Lewis lung carcinoma after exposure to cobalt-60 gamma rays *Radiat. Res.* 149 98-102
- Wieland D M, Wu J, Brown L E, Mangner T J, Swanson DP, and Bierwaltes W H 1980 Radiolabelled adrenergic neuron-blocking agents: adrenomedullary imaging with [¹³¹I]iodobenzylguanidine *J. Nucl. Med.* 21 349-353